Monatsh Chem (2015) 146:449–458
DOI 10.1007/s00706-014-1311-9

ORIGINAL PAPER

Functional monomer screening and preparation of dibenzothiophene-imprinted polymers on the surface of carbon microsphere

Lei Qin · Weifeng Liu · Yongzhen Yang · Xuguang Liu

Received: 2 July 2014 / Accepted: 7 September 2014 / Published online: 24 September 2014

Abstract Three candidate monomers (methacrylic acid, 2-vinyl pyridine, and 2-acrylamide-2-methyl sulfuric acid) were screened through computational simulation method to prepare effective surface molecularly imprinted polymers (SMIPs) based on carbon microspheres (CMSs) for dibenzothiophene removal from fuels. The optimized structures of complexes were described using density functional theory calculation at B3LYP/6-311++G(d,p) level and frequency calculations for each molecule and complex were conducted to provide insights into electrostatic interaction between monomers and template DBT. Besides, the reliability of computational simulation method for screening was tested by comparing the theoretical data with experimental results from gas chromatography. The computational data suggest that methacrylic acid (MAA) was the preferred monomer with the largest absolute binding energy (14.79 kJ mol^{-1}), which is in accordance with the experimental results. Thesaturated adsorption of PMAA-SMIPs/CMSs was the best (41.73 mg g^{-1}). Besides, PMAA-SMIPs/CMSs show highest special selectivity for dibenzothiophene against benzothiophene, and the relative selectivity coefficient k' was 2.02. The computational simulation method can be effectively used in monomer screening. This work may help understand the mechanisms of polymerization and recognition process between SMIPs and template and design SMIPs with improved adsorption performance.

Keywords Surface molecularly imprinted polymers · Adsorption desulfurization · Nanostructures · Density functional theory · Computational chemistry · Gas chromatography

L. Qin · W. Liu · X. Liu (✉)
Key Laboratory of Interface Science and Engineering in Advanced Materials, Ministry of Education, Taiyuan University of Technology, Taiyuan, China
e-mail: liuxuguang@tyut.edu.cn

L. Qin · W. Liu · X. Liu
College of Chemistry and Chemical Engineering, Taiyuan University of Technology, Taiyuan, China

Y. Yang (✉)
Research Center on Advanced Materials Science and Technology, Taiyuan University of Technology, Taiyuan, China
e-mail: yyztyut@126.com

Introduction

Polyaromatic sulfur-containing compounds such as dibenzothiophene (DBT), benzothiophene, and their alkyl derivatives, which exist in fuels, are valuable intermediates in several organic and medicine synthesis processes. Combustion of these sulfur-containing compounds in petroleum and gasoline, on one hand, causes SO_x emission, which brings environmental problems such as acid rain, haze harassment, catalyst poisoning, and equipment corrosion [1]. On the other hand, DBT and its alkyl derivatives are destructed and wasted. Therefore, searching an effective way for deep desulfurization without breaking sulfur-containing molecules in fuels is urgently needed [2, 3]. Traditional ways for desulfurization include hydrodesulfurization, oxidative desulfurization [4], adsorptive desulfurization [5–7], extractive desulfurization [8], and biodesulfurization [9, 10]. These ways can hardly decrease sulfur content to the ever-stringent emission standard or they will destroy the sulfur-containing compounds that should have been retained and effectively utilized. Beyond these traditional ways, molecular imprinting technique

provides an alternative method for deep desulfurization of fuel oils and collecting the sulfur compounds at the same time. Because of its high efficiency on selectively removing the refractory sulfur compounds under mild operation conditions and its environmentally friendly properties [8], molecular imprinting technique has drawn a wide attention around the world [11–13].

For desulfurization, molecularly imprinted polymers (MIPs) [14] are excellent adsorbents with several unique advantages since their memory effect of the size, shape, and functional groups of the template molecules [15, 16]. Thus, MIPs can be used to enrich, separate, and purify polyaromatic sulfur-containing compounds from fuels [17, 18]. Furthermore, in recent years, surface molecularly imprinted polymers (SMIPs), which are constructed on the surface of supports [19–21], are very attractive for adsorptive desulfurization. Identical sites of SMIPs are distributed on the surface of supports, for this reason, mass transfer is accelerated and binding capacity is improved [16, 22]. SMIPs based on various functional materials, such as SiO_2 [23], TiO_2 [24], grapheme [25], carbon nanotubes [26], and carbon microspheres (CMSs) have been reported. Among the various options, CMSs are one of the ideal support materials for their good thermal stability, excellent mechanical performance, and acid/base resistance [27]. Recently, Yang et al. [14] obtained the molecularly imprinted materials on the surface of CMSs with adsorption capacity towards DBT 109.5 mg g^{-1}. Liu et al. [28] prepared double-template MIPs on the surface of CMSs.

Besides the supports, monomer screening is another vital factor that determines adsorption performance of SMIPs, for the reason that adsorption of SMIPs largely depends on the interaction between template and functional monomers [29–31]. The formation of template–monomer complex is the basis for the molecular memory of SMIPs. Thus, the more stable the complex is, the more effective SMIPs will perform [39]. Up to now, finding and synthesizing functional monomers [14, 32] bring difficulties for selecting an effective monomer for certain template through an empirical way, which is time consuming and not pragmatic [33, 34]. Hence, many other methods are developed for screening functional monomers such as computer simulation [34], ultraviolet [35], nuclear magnetic resonance [36], and fluorescent spectroscopy [37].

In this research, candidate monomers methacrylic acid (MAA), 2-vinyl pyridine (2-VP), and 2-acrylamide-2-methyl sulfuric acid (AMPS) were selected through computational simulation to prepare effective adsorbent SMIPs for DBT removing from fuels. Besides, the reliability of computational screening method was tested by comparing the computational data with experimental results from gas chromatography (GC). According to the computational simulation, complex DBT-MAA processes largest binding energy and the GC experimental results that the PMAA-SMIPs/CMSs performed best in removing DBT, which inspected the validity computational method for monomers screening. This work may help gradually understand the mechanisms of recognition process of DBT on SMIPs and design SMIPs with improved selectivity and adsorption capacity.

Results and discussion

Computational monomer screening: optimized structure of DBT

Theoretical model of DBT is the most reasonable model with the lowest energy. Through computational simulation method the most reasonable model of DBT was optimized by density functional theory (DFT) method at B3LYP employing 6–311++G(d,p) level [38, 39] and the structure is shown as Fig. 1. DBT is a heterocyclic sulfur compound that contains two hexa-atomic rings and a five-membered

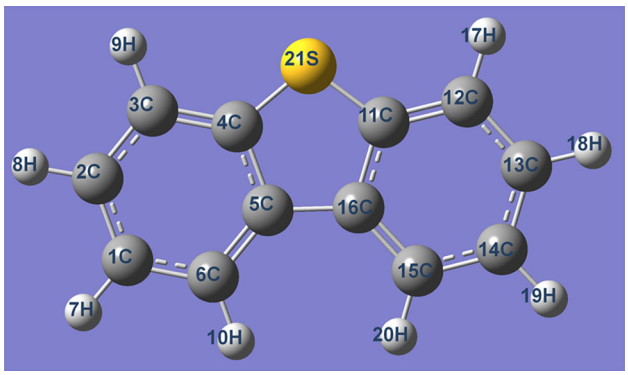

Fig. 1 The structure of DBT molecule with atomic numbering

Table 1 Optimized and experimental geometries of DBT molecule

Bond length/nm	Calc.	Exp.	Bond angle/°	Calc.	Exp.
R(1C–2C)	0.1402	0.1385	∠(1C–2C–3C)	120.7	121.6
R(2C–3C)	0.1390	0.1384	∠(2C–3C–4C)	118.5	117.8
R(3C–4C)	0.1395	0.1386	∠(3C–4C–5C)	121.7	121.6
R(4C–5C)	0.1411	0.1409	∠(4C–5C–6C)	118.7	118.7
R(5C–6C)	0.1402	0.1392	∠(5C–6C–1C)	119.8	120.0
R(6C–1C)	0.1388	0.1370	∠(6C–1C–2C)	120.6	120.5
R(4C–21S)	0.1765	0.174	∠(3C–4C–21S)	126.0	126.1
R(5C–16C)	0.1454	0.1441	∠(5C–4C–21S)	112.3	112.3
R(3C–9H)	0.1084		∠(4C–21S–11C)	91.0	91.5
R(2C–8H)	0.1084		∠(4C–5C–16C)	112.2	111.9
R(1C–7H)	0.1084		∠(6C–5C–16C)	129.1	129.4
R(6C–10H)	0.1084				

ring. Besides, it shows C_{2v} symmetry. According to the lengths and angles of its bonds (Table 1), it can be found that the planar construction of DBT is similar to that of benzene [40]. The optimized geometries of DBT match well with the experimental data.

Based on the optimized DBT model, the theoretical frequencies of DBT molecule (Fig. 2a) were calculated and compared with the experimental results (Fig. 2b). According to theoretical calculations, the Fourier transform infrared spectrometer (FT-IR) spectrum of DBT shows the strong absorption band at 728 cm^{-1} attributing to the out-of-plane bending vibration of –CH on benzene rings. The absorption at 3,091 cm^{-1} is caused by stretching vibration of C–H bond. The absorption around 1,406 cm^{-1} is the result of thiophene ring vibration. Correspondingly, the experimental results shows that the bending vibration of –CH on benzene rings is at 725 cm^{-1}, the stretching vibration of C–H bond is at 2,960 cm^{-1}, and thiophene ring vibration is at around 1,465 cm^{-1}. The differences are aroused since the molecules in real solid-state DBT are not free to move and the molecules are affected with each other. The computational frequencies resemble well with the experimental results. Thus, the computational method could be a promising tool for description of the complex system.

Monomer screening

Based on the theoretical and experimental analysis above, the optimized conformations of DBT, MAA, 2-VP, and AMPS are presented in Fig. 3. With the lowest energy principle, optimized conformations of the complexes DBT-MAA, DBT-2-VP, and DBT-AMPS were simulated as presented in Fig. 4.

The results in Table 2 demonstrate the energy *E*/a.u. of template DBT and monomers (MAA, 2-VP, AMPS) as well as the binding energy ΔE/a.u. of DBT-MAA, DBT-2-VP, and DBT-AMPS. It is obvious that all these three monomers can be bound with DBT to form stable complexes. The stable geometry of complexes indicates that there are interactions between DBT and these monomers. The binding energy of DBT-MAA is the lowest (-14.797 kJ mol^{-1}) and the binding energy of DBT-2-VP is the highest (-4.014 kJ mol^{-1}), which reveals that MAA is the most preferred monomer for DBT identification and the 2-VP is the least favorable one.

Interactions between DBT and each monomer

The nature of interactions between template and monomers can be discussed through investigations on changes before

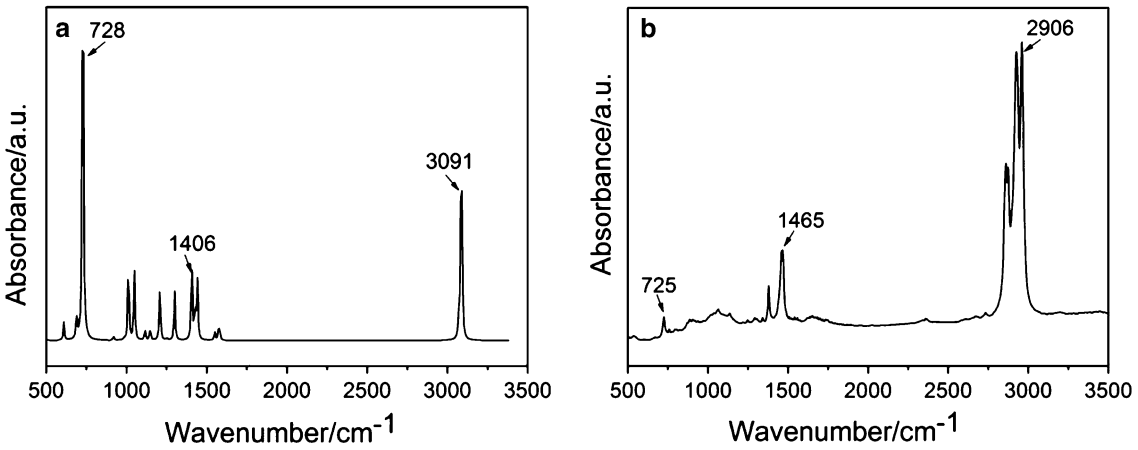

Fig. 2 Theoretical FT-IR spectrum for DBT molecule (**a**) and experimental FT-IR spectrum for DBT in solid (**b**)

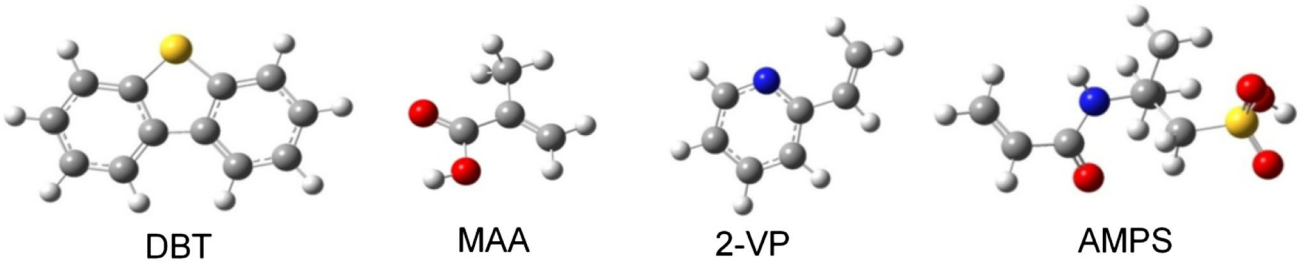

Fig. 3 The optimized structures of DBT, MAA, 2-VP, and AMPS molecules

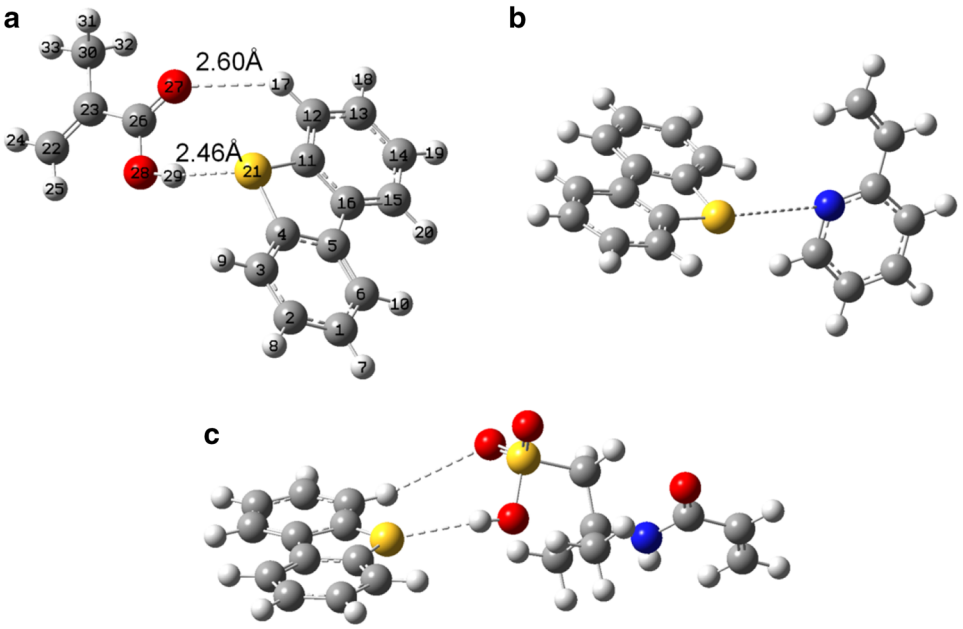

Fig. 4 The structures of the complexes: DBT-MAA (**a**), DBT-2-VP (**b**), DBT-AMPS (**c**)

Table 2 Binding energy of template-functional monomer

Molecule	*E*/a.u.	Δ*E*/a.u.	Δ*E*/kJ mol^{-1}
DBT	−860.444415	–	
MAA	−306.582172	–	
2-VP	−325.774337	–	
AMPS	−1028.560117	–	
DBT-MAA	−1167.032223	−0.005635	−14.79
DBT-2-VP	−1186.220281	−0.001528	−4.012
DBT-AMPS	−1889.008758	−0.004225	−11.093

1 a.u. = 2625.499748 kJ mol^{-1}

and after the combinations of DBT and monomers. Overlapped FT-IR spectra of DBT and MAA are shown as Fig. 5a, and the FT-IR spectrum of DBT-MAA is shown as Fig. 5b. The stretching vibration of –OH moved from 3,654 to 3,484 cm^{-1} with increased absorption intensity after compounding. The out-of-plane bending vibration of –OH at 550 cm^{-1} for MAA disappears in spectrum of DBT-MAA. Besides, the stretching vibration of C=O shifted from 1,723 to 1,706 cm^{-1} and out-of-plane vibration of C–O–H from 1,102 to 1,126 cm^{-1}. The changes in locations and intensities of characteristic absorption bands indicate the interactions, for instance electrostatic interaction and hydrogen bond interaction, include between DBT and MAA.

Electric charge distribution is an important factor that influences interactions between molecules. The natural bond orbital (NBO) charges of atoms belonging to MAA, DBT, or DBT-MAA are listed in Table 3. After compounding, the atomic charges rearranged. For instance, the

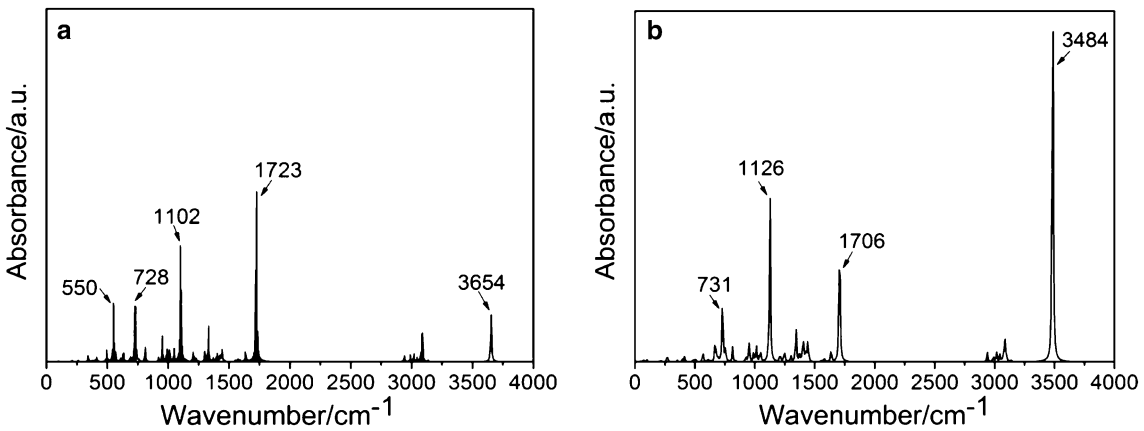

Fig. 5 The overlapped FT-IR spectra of DBT and MAA (**a**) and FT-IR spectrum of DBT-MAA complex (**b**)

Table 3 Atomic charges for DBT and MAA before and after compounding

No.	Atom	Atomic charge/a.u.	
		Individual	Complex
MAA			
26	C	0.773	0.779
27	O	−0.596	−0.614
28	O	−0.691	−0.699
29	H	0.485	0.490
DBT			
21	S	0.387	0.355
11	C	−0.156	−0.150
12	C	−0.201	−0.202
13	C	−0.200	−0.195
14	C	−0.208	−0.203
15	C	−0.173	−0.176
16	C	−0.088	−0.087
17	H	0.212	0.236
4	C	−0.166	−0.163
5	C	−0.066	−0.062

negative charge of C(26) in complex decreased by 0.006, while the negative charge of O(28) increased by 0.008. During the compounding process, the charges shifted from DBT to MAA, which indicate the electrostatic interaction between DBT and MAA [41].

Additionally, hydrogen bond also strengthens the interaction between DBT and MAA. Through the establishment of O–H bond, O(27) (−0.596) in MAA and H(17) (0.212) in DBT were considerably influenced. Furthermore, hydrogen bond C=O···H–C affected the space structure of DBT-MAA complex. At the same time, changes of charge on S(21) and H(29) indicated the formation of C–S···H–O. These hydrogen bonds affected FT-IR absorption significantly. Characteristic absorption peaks of –C=O and –OH of DBT-MAA were shifted to the region of low wavenumber.

Unlike the interactions between DBT and MAA, the interactions between DBT and 2-VP were very weak. The FT-IR spectrum of DBT-2-VP had little differences with the overlapped FT-IR spectra of DBT and 2-VP, as shown in Fig. 6. The weak interaction between DBT and 2-VP was clearly due to the lack of hydrogen bonds between them.

Corresponding analysis on DBT, AMPS and their complex DBT-AMPS was carried out. As shown in Fig. 7a, plenty functional groups of AMPS gave the complicated absorption spectra. The stretching vibrations of O=S=O, C=O, and –OH of AMPS were at 1,353, 1,723, and 3,772 cm^{-1}, respectively. According to the FT-IR spectrum of DBT-AMPS (Fig. 7b), the stretching vibrations of O=S=O and C=O shifted to 1,299 and 1,727 cm^{-1}, respectively, with the decrease in absorption intensity. At the same time, out-of-plane vibration of =CH in DBT (728 cm^{-1}) shifted to 731 cm^{-1} in DBT-AMPS. Similar to the case of MAA, the hydrogen bond in DBT-AMPS improved the stability of the complex.

Characterization of SMIPs/CMSs

The SMIPs/CMSs with different monomers have similar morphological structures. Here the FESEM images and thermogravimetric analysis (TGA) curves of SMIPs/CMSs with MAA as its monomer are provided to illustrate the morphological structures and thermal stability of SMIPs/CMSs [42]. The CMSs with uniform size agglomerated partly, as shown in Fig. 8a. After polymerization, CMSs were covered by a shell of polymer and better dispersed (Fig. 8b). The content of polymer on the surface of CMSs was measured by TGA, as shown in Fig. 8c. CMSs had a small weight loss

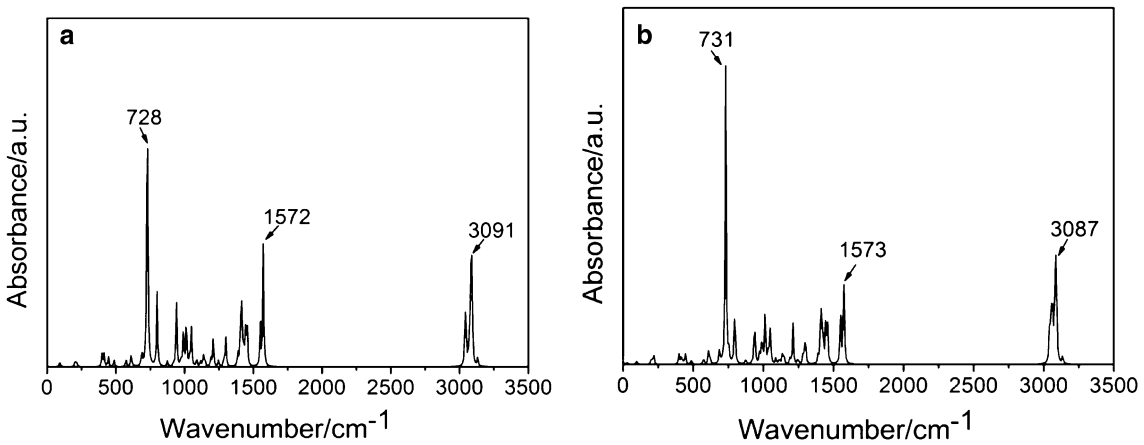

Fig. 6 The overlapped FT-IR spectra for DBT and 2-VP (**a**) and FT-IR spectrum for the complex of DBT-2-VP (**b**)

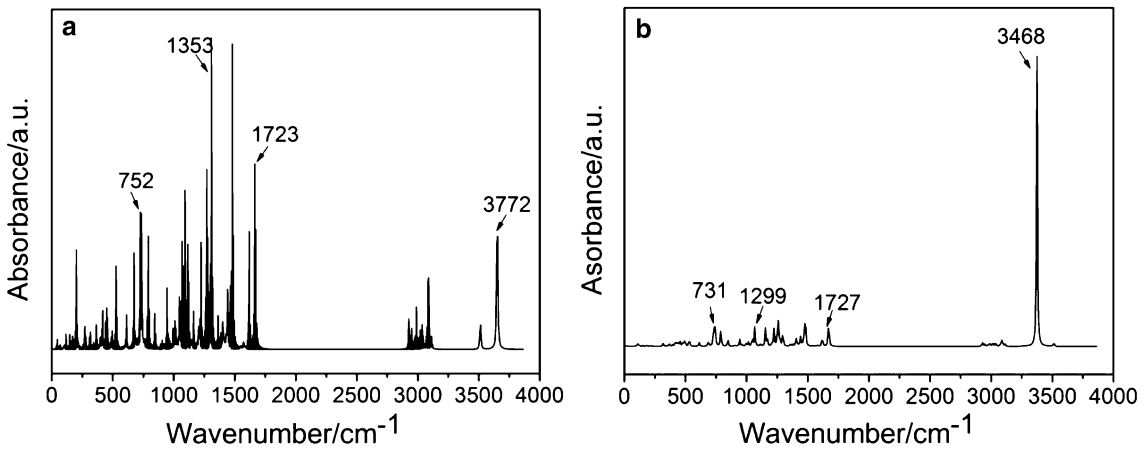

Fig. 7 The overlapped FT-IR spectra for DBT and AMPS (**a**) and FT-IR spectrum for the complex of DBT-AMPS (**b**)

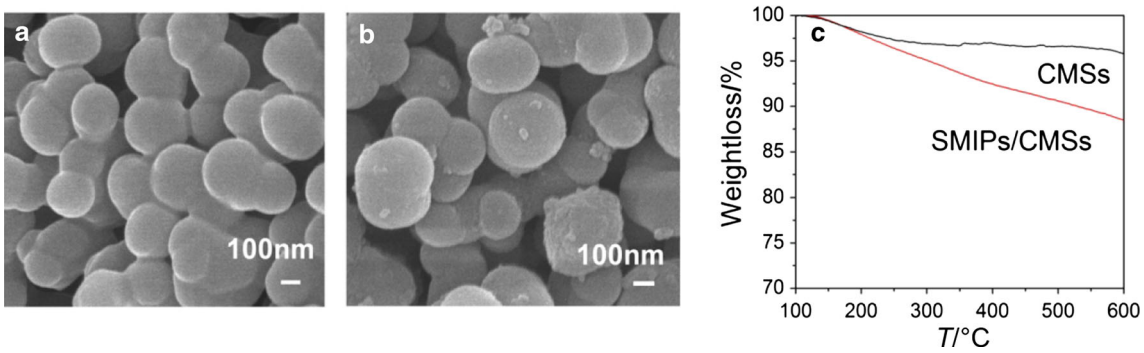

Fig. 8 FESEM images of CMSs (**a**), SMIPs/CMSs (**b**); TG curves of CMSs and MIP/CMSs (**c**) (TG conditions: 10 °C min^{-1}, N_2)

between 100 and 200 °C, which is attributed to release of short chain organics on the surface of CMSs, while SMIPs/CMSs degraded still evidently after 200 °C, attributed to decomposition of MIPs-layer with the final weight of 88.4 % at 600 °C. The difference in the weight loss at 600 °C between SMIPs/CMSs and CMSs suggests that the grafting content of SMIPs on CMSs is 7.4 %.

Adsorption kinetics

The capacity of adsorption can be measured by kinetic adsorption performance. The kinetic adsorption curves of SMIPs/CMSs and non-imprinted polymers on CMSs (NIPs/CMSs) toward DBT are shown in Fig. 9. The trends of the adsorption for three kinds of SMIPs/CMSs with different monomers were alike. The adsorption amount of DBT increased with time and finally reached saturation. SMIPs/CMSs had a higher DBT adsorption capacity of DBT than NIPs/CMSs, implying that MIPs-layer was grafted onto the surface of CMSs. In other words, the results indicate that SMIPs/CMSs with specific recognition sites had higher binding affinity for DBT. For each products PMAA-SMIPs/CMSs, P(2-VP)-SMIPs/CMSs, and PAMPS-SMIPs/CMSs, the GC results indicate that the adsorption equilibrium time was about 240, 120, and 180 min; the saturated adsorption amount was 41.73, 23.26, and 20.25 mg/g; the imprinting factor (IF = q_e(SMIPs)/q_e(NIPs)) was 1.52, 1.71, and 1.28, respectively. The imprinting can be considered as effective when the imprinting factor is >1.5 [54]. It is obvious that PMAA-SMIPs/CMSs and P(2-VP)-SMIPs/CMSs are effectively imprinted.

Although NIPs/CMSs had not so many specific sites for recognizing DBT, the retention of DBT on NIPs/CMSs seemed to be a good estimation of the interaction of functional monomers with template DBT [30]. Since complex DBT-MAA owns the highest binding energy, the adsorption capacity of PMAA-NIPs/CMSs is the best. While the least binding energy of DBT-2-VP leads the worst adsorption performance of P(2-VP)-NIPs/CMSs.

Adsorption selectivity

Adsorption selectivity is another important factor to evaluate the adsorbents. The selectivity of SMIPs/CMSs and NIPs/CMSs towards DBT was studied by competitive experiments. According to Fig. 10, SMIPs/CMSs perform

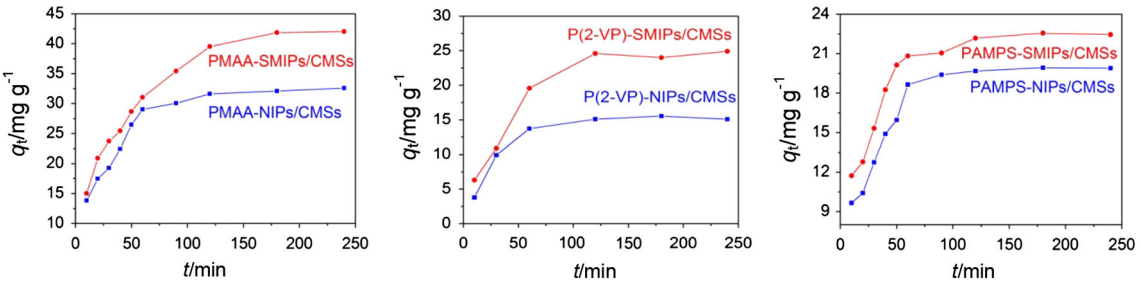

Fig. 9 Kinetic adsorption curves of SMIPs/CMSs and NIPs/CMSs for DBT (15 mg of SMIPs/CMSs or NIPs/CMSs, 10 cm^3 of 500 mg dm^{-3} DBT in *n*-hexane, 25 °C)

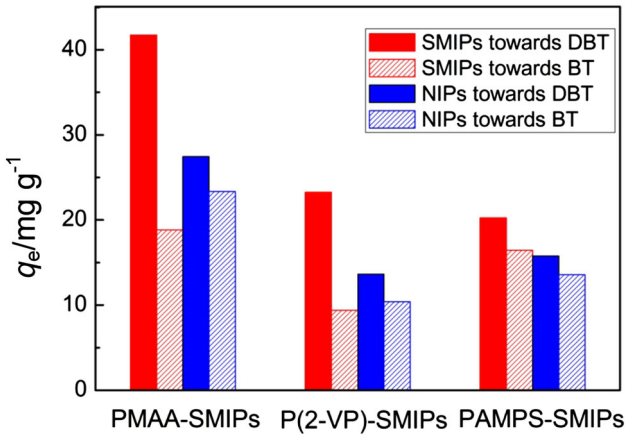

Fig. 10 The competitive adsorption of DBT and BT onto SMIPs/CMSs and NIPs/CMSs

better adsorption capacity and selectivity than NIPs/CMSs. DBT can be identified more easily than benzothiophene (BT) since the monomers were chosen directly for DBT, and the imprinted sites on SMIPs/CMSs did not match well with BT, although they possess similar structures. Among these three SMIPs/CMSs, PMAA-SMIPs/CMSs exhibited excellent adsorption capacity and selectivity towards DBT.

The values of $q_{e,DBT}$, $q_{e,BT}$, k_d, k, and k' are summarized in Table 4. Value k of SMIPs/CMSs and NIPs/CMSs indicates the specific affinity towards DBT with respect to BT. Value k' indicates that the higher selectivity of SMIPs/CMSs for extraction of DBT than that of NIPs/CMSs. Thus, among these three SMIPs/CMSs, PMAA-SMIPs/CMSs ($k' = 2.02$) performed best in selective adsorption.

SMIPs/CMSs with MAA, 2-VP, and AMPS as functional monomer were prepared separately. The computational binding energy and GC adsorption results are listed in Table 5. It can be seen that the experimental results agree well with the calculational data. The adsorption value of SMIPs/CMSs with MAA as functional monomer towards DBT was 41.73 mg g^{-1}, exceeding the values of the SMIPs using 2-VP or AMPS as monomer, which reached 23.26 and 20.25 mg g^{-1}, respectively. These experimental results have been predicted by the highest absolute amount of binding energy (14.79 kJ mol^{-1}). Thus, MAA was obviously superior to 2-VP and AMPS for DBT-imprinted polymers.

There were some inevitable differences in the solvent, temperature, dosage of reagents during synthesis of SMIPs/CMSs with these three functional monomers and the following processes of removing DBT, though the overall synthesis procedure was the same. Therefore, the resultant SMIPs probably possessed different density of recognition sites, different degree of site heterogeneity, and different physical environments around the sites, which would directly lead to different binding capacity and binding kinetics of SMIPs towards DBT. Thus, further experiments are needed for clearer elucidation of the recognition mechanism of SMIPs/CMSs towards DBT.

Conclusions

Based on DFT method, the stable complex structure was optimized using B3LYP at 6-311++G(d,p) level and investigation of vibrational frequencies enhanced

Table 4 The competitive adsorption of DBT and BT onto SMIPs/CMSs and NIPs/CMSs

Polymer	$q_{e,DBT}$/mg g^{-1}	$q_{e,BT}$/mg g^{-1}	$k_{d,DBT}$/cm^3 g^{-1}	$k_{d,BT}$/cm^3 g^{-1}	k	k'
PMAA-SMIPs/CMSs	41.73	18.84	95.40	56.11	1.70	2.02
PMAA-NIPs/CMSs	27.46	23.34	59.85	70.94	0.84	–
P(2-VP)-SMIPs/CMSs	23.26	9.38	50.26	26.88	1.87	1.97
P(2-VP)-NIPs/CMSs	13.64	10.41	28.44	29.88	0.95	–
PAMPS-SMIPs/CMSs	20.25	16.47	43.12	48.54	0.89	1.06
PAMPS-NIPs/CMSs	15.76	13.58	33.08	39.52	0.84	–

Table 5 The recognition and selective ability of MIP with different functional monomers towards DBT

Sample	Equilibrium time/min	Saturated adsorption for DBT/mg g^{-1}	Relative selectivity (k')	ΔE/kJ mol^{-1}
PMAA-SMIPs/CMSs	240	41.73	2.02	−14.79
P(2-VP)-SMIPs/CMSs	120	23.26	1.97	−4.012
PAMPS-SMIPs/CMSs	180	20.25	1.06	−11.09

Scheme 1

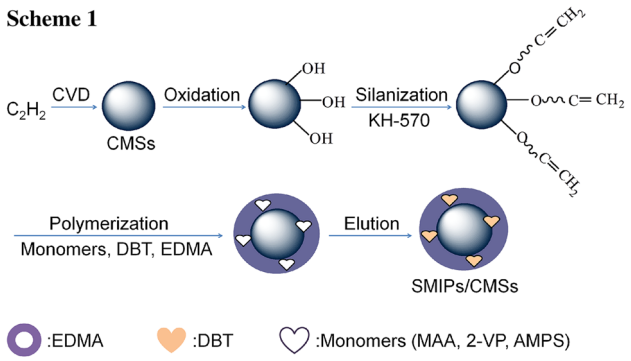

understandings of electrostatic interaction underlying the formation of the complex of DBT and monomers MAA, 2-VP, and AMPS. The complex DBT-MAA processes largest absolute binding energy (14.79 kJ mol^{-1}), which indicates the superiority of MAA. Then the effective SMIPs were synthesized on the surface of CMSs. The SMIPs/CMSs were shelled by a layer of DBT-imprinted polymer on the surface of CMSs and showed good dispersion. The kinetic adsorption results indicate that among these three kinds of SMIPs/CMSs, the equilibrium time and the saturation adsorption of PMAA-SMIPs/CMSs were best (240 min, 41.73 mg g^{-1}). Besides, PMAA-SMIPs/CMSs showed highest special selectivity for DBT with respect to BT, and the relative selectivity coefficient k' was 2.02. The GC results agree well with the computational data. The computational simulation method can be effectively used in monomer screening for the preparation of SMIPs with excellent adsorption performance.

Experimental

CMSs (~300 nm in diameter) were prepared by chemical vapor deposition (CVD) using C_2H_2 as carbon source. H_2SO_4 and HNO_3 were obtained from Taiyuan Fertilizer Factory Chemical Reagent Factory, Taiyuan, China. 3-(Methacryloxypropyl)trimethoxysilane (KH-570), ethylene dimethacrylate (EDMA, 98 %), DBT (98 %), 2-VP, AMPS, and BT (≥98 %) were obtained from Alfa Aesar, USA. MAA was obtained from Chemical Reagent Company of Tianjin University, China. Azoisobutyronitrile (AIBN) was obtained from Shanghai Shisihewei Chemical Engineering Co. Ltd, Shanghai, China. All other chemicals were of analytical grade. Deionized water was used to prepare all buffers and solutions.

Computational simulation

The molecular structures of template DBT, functional monomers MAA, 2-VP, AMPS, and their complex (DBT-MAA, DBT-2-VP, DBT-AMPS) were initially optimized with a semi-empirical method using Austin Model 1 (AM1). Further theoretical investigations were performed by DFT method using the hybrid density functional B3LYP. Geometry optimizations and frequency calculations of single molecule and complex were performed at the B3LYP/6-311++G(d,p) level. Calculations presented in this study were carried out applying Gaussian 09 program package [38, 39].

SMIPs/CMSs preparation

The SMIPs/CMSs towards DBT was prepared through a molecular imprinting route, as shown in Scheme 1. CMSs (~300 nm) were synthesized by CVD with C_2H_2 as carbon source and Ar as carrier gas. The synthesized CMSs were modified by H_2SO_4 and HNO_3 (3:1 v/v) to introduce hydroxyl groups. Then the C=C functional groups were grafted on the surface of oxidized CMSs by reaction with silane coupling agent KH-570. After that, the template DBT (1 mmol) was dissolved in 10 cm^3 of ethanol and monomer MAA, 2-VP, or AMPS (4 mmol) was dissolved in 10 cm^3 of dimethylformamide (DMF), respectively. The reagents in solution were well interacted under magnetic stirring for 1 h. Then 0.1 g silanized CMSs and 16 mmol EDMA were added. The mixture was ultrasonically dispersed for 5 min. Finally, DMF solution (5 cm^3) of 0.01 g of initiator AIBN was added dropwise for uniform polymerization. The polymerization process lasted 24 h at 70 °C.

The resultant products were washed by centrifuging at 8000 rpm using acetic acid/ethanol composed solution (1:9 v/v) to remove impurities and elute DBT from the polymer matrix. The dried products were soaked in 200 cm^3 *n*-hexane with magnetic stirring for 12 h to further remove template DBT from recognition sites. At last, SMIPs/CMSs were obtained by centrifuging and drying at 50 °C for 20 h.

The amount of eluted DBT was monitored by gas chromatography (GC). The non-imprinted analog NIPs/CMSs were prepared through the same process just without adding DBT as template.

Adsorption performance of SMIPs/CMSs

Static adsorption experiments

SMIPs/CMSs (15 mg) (or NIPs/CMSs) were introduced into the centrifuge tube with 10 cm^3 of DBT solution in *n*-hexane (simulate oil solution, $C_0 = 500$ mg dm^{-3}). Then, the adsorption process was kept steadily with magnetic stirring at 25 °C. At different time interval, the concentration (C_t/mg dm^{-3}) of DBT solution was tested by the GC. The adsorption capacity of DBT (q_t/mg g^{-1}) was calculated according to Eq. (1), where *V*/*L* is the volume of the DBT solution; *m*/g is the mass of SMIPs/CMSs or NIPs/CMSs.

$$q_t = \frac{V(C_0 - C_t)}{m} \quad (1)$$

Competitive adsorption experiments

In order to study the selectivity of SMIPs/CMSs towards DBT, BT was selected as interferent owing to its similar structure with DBT. The mixture of DBT and BT was prepared with the same concentration of 500 mg dm^{-3}. Then the static adsorption experiments were conducted for the mixture solution. After the adsorption equilibrium was reached, the concentrations of DBT and BT were detected by GC. The selectivity of NIPs/CMSs toward DBT was also performed in the same procedure.

The distribution coefficients of DBT and BT were calculated by Eq. (2) [31], where k_d/cm^3 g^{-1} is the distribution coefficient; q_e/mg g^{-1} is the equilibrium adsorption capacity; C_e/mg cm^{-3} is the equilibrium concentration.

$$k_d = \frac{q_e}{C_e} \quad (2)$$

The selectivity coefficients of SMIPs/CMSs and NIPs/CMSs for DBT were obtained from the distribution coefficient k_d according to Eq. (3).

$$k = \frac{k_{d(DBT)}}{k_{d(BT)}} \quad (3)$$

The value of relative selectivity coefficient k' was defined as Eq. (4), indicating the enhanced extent of the selectivity of SMIPs/CMSs for DBT with respect to NIPs/CMSs.

$$k' = \frac{k_{(SMIPs/CMSs)}}{k_{(NIPs/CMSs)}} \quad (4)$$

Acknowledgments We are grateful to National Natural Science Foundation of China (21176169), Shanxi Provincial Key Innovative Research Team in Science and Technology (2012041011), International Science and Technology Cooperation Program of China (2012DFR50460) and Shanxi Scholarship Council of China (2012-038) for financial support.

References

1. Ania CO, Bandosz TJ (2005) Langmuir 21:7752
2. Seredych M, Wu CT, Brender P, Ania CO, Vix-Guterl C, Bandosz TJ (2012) Fuel 92:318
3. Tao H, Nakazato T, Sato S (2009) Fuel 88:1961
4. Zhang J, Wang AJ, Li X, Ma Xuehu (2011) J Catal 279:269
5. Yu C, Fan XM, Yu LM, Bandosz T, Zhao ZB, Qiu JS (2013) Energy Fuels 27:1499
6. Xu X, Shen XP, Zhu GX, Jing LQ, Liu XS, Chen KM (2012) Chem Eng J 200:521
7. Seredych M, Bandosz TJ (2010) Energy Fuels 24:3352
8. Asumana C, Yu GR, Li X, Zhao JJ, Liu G, Chen XC (2010) Green Chem 12:2030
9. Davoodi-Dehaghani F, Vosoughi M, Ziaee AA (2010) Bioresour Technol 101:1102
10. Dinamarca MA, Ibacache-Quiroga C, Baeza P, Galvez S, Villarroel M, Olivero P, Ojeda J (2010) Bioresour Technol 101:2375
11. Byrne ME, Salian V (2008) Int J Pharm 364:188
12. Castro B, Whitcombe MJ, Vulfson EN, Vazquez-Duhalt R, Barzana E (2001) Anal Chim Acta 435:83
13. Haupt K, Mosbach K (2000) Chem Rev 100:2495
14. Yang YZ, Liu XG, Guo MC, Li S, Liu WF, Xu BS (2011) Colloids Surf A 377:379
15. Shen X, Zhu L, Wang N, Ye L, Tang H (2012) Chem Commun 48:788
16. Chen LX, Xu SF, Li JH (2011) Chem Soc Rev 40:2922
17. Mathew-Krotz J, Shea KJ (1996) J Am Chem Soc 118:8154
18. Gao BJ, Wang J, An FQ, Liu Q (2008) Polymer 49:1230
19. Lee HY, Kim BS (2009) Biosens Bioelectron 25:587
20. Zhao WH, Sheng N, Zhu R (2010) J Hazard Mater 179:223
21. Chi WH, Shi HG, Shi W, Guo Y, Guo TY (2012) J Hazard Mater 227–228:243
22. Xie CG, Zhang ZP, Wang DP, Guan GJ, Gao DM, Liu JH (2006) Anal Chem 78:8339
23. Hu TP, Zhang YM, Zheng LH (2010) J Fuel Chem Technol 38:722
24. Xu WZ, Zhou W, Xu PP, Yan YS, Wu XY (2011) Chem Eng J 172:191
25. Duan FF, Chen CQ, Wang GZ, Yang YZ, Liu XG, Qin Y (2014) RSC Adv 4:1469
26. Morishita T, Matsushita M, Katagiri Y (2009) Carbon 11:2716
27. Serp P, Feurer R, Kalck P (2001) Carbon 39:621
28. Liu WF, Liu XG, Yang YZ, Zhang Y, Xu B (2014) Fuel 117:184
29. Zeng H, Wang YZ, Liu XJ, Kong JH, Nie C (2012) Talanta 93:172
30. Nicholls IA, Adbo K, Andersson HS, Andersson PO, Hedin-Dahlstrom J, Jokela P, Karlsson JG, Olofeeon L, Rosengren J, Shoravi S, Svenson J, Wikman S (2001) Anal Chim Acta 435:9
31. Karim K, Breton F, Rouillon R, Piletska EV, Guerreiro A, Chianella I, Piletsky (2005) Adv Drug Delivery Rev 57:1795
32. Yong YZ, Zhang Y, Li S, Liu XG, Xu BS (2012) Appl Surf Sci 258:6441
33. Yao JH, Li X, Qin W (2008) Anal Chim Acta 610:282
34. Dong C, Li X, Guo Z, Oi J (2009) Anal Chim Acta 647:117

35. Li P, Rong F, Zhu XL, Hu RJ, Yuang CW (2003) Acta Polym Sin 724
36. Farrington K, Regan F (2007) Biosens Bioelectron 22:1138
37. Su LQ, Zhang XL, Liang YK (2009) Chemistry 749
38. Saloni J, Lipkowski P, Dasary SR (2011) Polymer 52:1206
39. Prasad BB, Rai G (2012) Spectrochim Acta A 88:82
40. Lee SY (2001) J Phys Chem A 105:8093
41. Niu XQ, Zhang JG, Feng XJ, Chen PW, Zhang TL, Wang SY, Zhang SW, Zhou ZN, Yang L (2011) Acta Chim Sin 69:1627
42. Cheng WJ, Liu ZJ, Wang Y (2013) Talanta 116:396